Assessment of the acoustic scattering matrix of a heat exchanger using ssCFD-LNSE simulation

Assessment of the acoustic scattering matrix of a heat exchanger using ssCFD-LNSE simulation

Hamed F. Ganji[1]
Department of Mechanical Engineering, Eindhoven University of Technology, the Netherlands

Viktor Kornilov[2]
Department of Mechanical Engineering, Eindhoven University of Technology, the Netherlands

Jeroen van Oijen[3]
Department of Mechanical Engineering, Eindhoven University of Technology, the Netherlands

Ines Lopez Arteaga[4]
Department of Mechanical Engineering, Eindhoven University of Technology, the Netherlands
Department of Engineering Mechanics, KTH Royal Institute of Technology, Sweden

ABSTRACT

The risk of thermoacoustic instability is present in any combustion appliance. The instability results from a closed loop feedback between unsteady combustion, heat-transfer and acoustic modes of the system. To predict the system acoustics, all constituting elements of the appliance need to be modelled. A heat-exchanger is a element where the gas faces complex fluid dynamics and heat transfer processes. Therefore, modelling of (thermo)-acoustic properties of a heat exchanger is challenging. In this paper, a computational approach is proposed to characterize the acoustic properties of a generic heat exchanger in both laminar and turbulent flow regimes. A hybrid Computational Fluid Dynamics - Computational Aero-Acoustics (CFD-CAA) method is used based on the linearized Navier-Stokes equation, called ssCFD-LNSE. The core idea in this approach is to efficiently model acoustic wave propagation with inclusion of mean flow and temperature fields. ssCFD-LNSE is performed by splitting the quantities of the total field into a mean part (obtained from CFD) and a (acoustic) perturbation part modelled within the LNSE solver. The goal of this research is to assess the two-port acoustic scattering matrix of an array of tubes, as a generic model of a heat-exchanger, with a hot cross flow.

1. INTRODUCTION

In many ducted applications, such as domestic boilers, gas turbines, a direct acoustic simulation of thermoacoustics with current computers seems still unmanageable due to the overwhelming

[1]h.faghanpourganji@tue.nl

[2]v.kornilov@tue.nl

[3]j.a.v.oijen@tue.nl

[4]i.lopez@tue.nl

computational costs associated with this multi-scales phenomenon. An alternative approach is a strategy, called Network modeling. In this approach, elements of an on-study system individually need to be acoustically characterized. One can consider a component as a black box, where the acoustic plane waves enter and exit through a number of ports. The system is represented as a connected network of elements to model instability [1]. A generic combustion system is modeled by breaking it down into a sequence of elements such as duct sections, junctions, area jumps, chambers, burners with flames, and heat exchangers. The most common heat exchanger configurations contain tube arrays inside cylindrical ducts. The heat-exchanger (HEX) not only scatters the acoustic waves due to the area and temperature variations, but also may generate aerodynamic and aeroacoustic effects (e.g. whistling because of flow-acoustic coupling). Therefore, the acoustic characterization of heat exchangers is quite complex due to the presence of different physical phenomenon. This is why the objective of this article is to assess the two-port acoustic scattering matrix of a generic model of a HEX.

There are relevant studies for the simplified cold HEX model with and without cross-flow. Quinn and Howe [2] studied acoustic propagation through a row of rigid strips and tubes in cold cross-flow. Huang and Heckl [3] considered a row of infinitely long, equally spaced tubes in the absence of cross flow, and by using the grating theory [4, 5] they found expressions for the reflection and transmission coefficients of this tube row. Dowling and Hughes [6] derived expressions for the reflection and transmission coefficient of a slit plate in cross-flow. Their formulation showed that the maximum absorption coefficient from an isolated slit screen greatly increased by placing a rigid surface behind the screen.

Surendran et al. [7] considered a single row of tubes with and without cold cross-flow. They used a quasi-steady model [8, 9] to superimpose a steady flow field to the acoustic field. The comparison with measurement showed that this frequency-independent theoretical model is plausible for low frequencies. Later, the influence of a laminar two-dimensional (2D) HEX to suppress combustion instabilities was studied using unsteady simulation with applying a step function perturbation, called system identification (SI) [10]. Surendran et al. modeled the HEX with an active heat sink using the transfer function technique. Since this work relies on system identification, it cannot provide detailed information on the propagation of the acoustic variable in the domain, and the use of the heat sink concept for the HEX limits the cases where the flame (heat source) is far enough away from HEX. This is the gap we are trying to fill with this work.

A hybrid Computational Fluid Dynamics - Computational Aero-Acoustics (CFD-CAA) method based on the fully linearized Navier-Stokes equation is used, called ssCFD-LNSE. The basic idea of this approach is to model the propagation of acoustic waves by including the mean flow field and the temperature effect. ssCFD-LNSE is performed by splitting the quantities of the total field into a mean part (obtained from steady-state CFD) and a perturbation part modelled within the LNSE solver [11]. This methodology has been used widely in linear ducted aeroacoustics and is of interest thanks to the significant reduction in computational cost. Recently, Na [12] used this approach to study a 2D turbulent flow around a cold HEX, and the results showed a good agreement against impedance tube measurements. The current work is an extension of their work for a generic hot heat-exchanger.

The paper is structured as follows. The ssCFD-LNSE methodology is described in section 2. This section is divided into three parts: First, the main features of the numerical approach used to obtain background information on the flow in laminar and turbulent cases are briefly summarized. Then, the considerations for mapping the CFD result to an acoustic mesh are presented, followed by the description of the LNSE. In Section 3, ssCFD-LNSE solver is validated using analytical models and experimental data. Then the application of the methodology to the generic 2D hot HEX is presented. Finally, conclusions are drawn in Section 4.

2. NUMERICAL METHODOLOGY: SSCFD-LNSE SOLVER

The full compressible Navier-Stokes equations for an ideal gas in the absence of any volume force can be written as:

$$\frac{\partial \rho}{\partial t} = -\nabla \cdot (\rho \mathbf{v}) \tag{1}$$

$$\rho \frac{\partial \mathbf{v}}{\partial t} = -\rho \mathbf{v} \cdot \nabla \mathbf{v} - \nabla p + \nabla \cdot \tau \tag{2}$$

$$\rho C_p \frac{\partial T}{\partial t} = \frac{\partial p}{\partial t} - \rho C_p \mathbf{v} \cdot \nabla T + \mathbf{v} \cdot \nabla p + \Psi + \nabla \cdot (K \nabla T) \tag{3}$$

These equations describe the fundamental conservation principles for mass, momentum and energy, respectively. The variables K, μ and C_p denote the thermal conductivity, dynamic viscosity and specific heat at constant pressure. ρ is density, $\mathbf{v}$ is velocity vector, T is the absolute temperature, and p is pressure and for an ideal gas $p = \rho R_0 T$, where R_0 is the universal gas constant. The Reynolds viscous stress tensor (τ) and the dissipation function (Ψ) can be defined as:

$$\tau = \mu_B (\nabla \cdot \mathbf{v}) \mathbf{I} + \mu [\nabla \mathbf{v} + (\nabla \mathbf{v})^T], \quad \Psi = \tau : (\nabla \mathbf{v})^T \tag{4}$$

where, μ_B is the bulk viscosity of the fluid. The ssCFD-LNSE method is based on this assumption that the influence of the acoustic disturbances on the mean velocity field is negligible, i.e., the steady velocity field can be determined independently. This assumption is valid in many applications in low mach number thermo- and aero-acoustics. In practice, this approach to obtain the two-port scattering matrix consists of three steps as described in the following sections:

2.1. Step1: Steady-state Computational Fluid Dynamic (ssCFD)

To obtain the background flow information, at the first step, a steady state flow simulation is performed. For the laminar flow, direct numerical simulation (DNS) is used, and the corresponding governing equation can be obtained easily by neglecting time derivatives terms in the fully compressible N-S equation (Eqs.1-3).

For high Reynolds number (Re), the steady state mean flow is simulated with a compressible Reynolds-Averaged Navier–Stokes (RANS) solver. In the present study, the shear stress transport (SST) two equation model [13], which has often been successfully employed for a broad range of applications, is employed to close the Reynolds stress tensor for turbulent flow.

$$\tau = -\frac{2}{3}(\mu + \mu_T)(\nabla \cdot \mathbf{v}) \mathbf{I} + (\mu + \mu_T)[\nabla \mathbf{v} + (\nabla \mathbf{v})^T] - \frac{2}{3} \rho \kappa \tag{5}$$

In this model, the following two equations are solved to obtain turbulent kinetic energy (κ) and specific dissipation rate (ω):

$$\rho (\mathbf{v} \cdot \nabla) \kappa = \nabla \cdot [(\mu + \mu_T \sigma_\kappa) \nabla \kappa] + P - \beta_0^* \rho \omega \kappa \tag{6}$$

$$\rho (\mathbf{v} \cdot \nabla) \omega = \nabla \cdot [(\mu + \mu_T \sigma_\omega) \nabla \omega] + \frac{\gamma}{\mu_T} \rho P - \rho \beta_0 \omega^2 + 2(1 - f_{v1}) \sigma_{\omega 2} \rho \nabla \kappa \cdot \nabla \omega - \beta_0 \rho \omega \kappa \tag{7}$$

With,

$$\mu_T = \rho \frac{a_1 \kappa}{\max(a_1 \omega, S f_{v2})} \tag{8}$$

$$f_{v1} = \tanh \left\{ \left\{ \min \left[\max \left(\frac{\sqrt{\kappa}}{\beta^* \omega y}, \frac{500 \mu}{\rho y^2 \omega} \right), \frac{4 \rho \sigma_{\omega 2} \kappa}{C D_{\kappa \omega} y^2} \right] \right\}^4 \right\}, \qquad f_{v2} = \tanh \left[\left[\max \left(\frac{2\sqrt{\kappa}}{\beta^* \omega y}, \frac{500 \mu}{\rho y^2 \omega} \right) \right]^2 \right] \tag{9}$$

$$P = \min(P_\kappa, 10\rho\beta_0\omega\kappa) \tag{10}$$

$$P_\kappa = \mu_T[\nabla\mathbf{v} : (\nabla\mathbf{v} + (\nabla\mathbf{v})^T) - \frac{2}{3}(\nabla\mathbf{v})^2] - \frac{2}{3}\rho\kappa\nabla\cdot\mathbf{v} \tag{11}$$

Where, P is the turbulent production, μ_T is the turbulent/eddy viscosity, y is the distance to the nearest wall, f_{v1} and f_{v2} are blending functions. $CD_{\kappa\omega}$ limited by $\max(2\rho\sigma_{\omega 2}\frac{1}{\omega}\nabla\kappa\cdot\nabla\omega, 10^{-10})$, and S is defined as $\sqrt{2\mathbf{S}:\mathbf{S}}$ for $\mathbf{S} = \frac{1}{2}(\nabla\mathbf{v} + (\nabla\mathbf{v})^T)$.

2.2. Step2: Mapping Between Fluid Flow and Acoustic Mesh

In most numerical cases, the CFD mesh and the (aero)acoustic mesh are two independent meshes with different resolutions due to different length scales, boundary layer considerations, etc. Therefore, the mapping of the CFD solution from the CFD mesh to the acoustic mesh should be done carefully to avoid introducing unwanted numerical effects into the acoustic solution. This mapping is performed using the *Background Fluid Flow Coupling* feature in COMSOL multiphysics. In the most general case, the variables for mean background flow pressure p_0, velocity field v_0, density ρ_0, temperature T_0, and turbulent viscosity μ_T should be mapped to the corresponding variables in the acoustic mesh. These mapped variables are then used as model inputs in the LNSE model.

2.3. Step3: Acoustic Propagation (LNSE solver)

The acoustic field is obtained by solving the linearized Navier-Stokes equations in the frequency domain, which are derived from the full compressible Navier-Stokes equations [11]. The equations are obtained according to the following procedure. The acoustic field obtained is cleaned of hydrodynamic pressure fluctuations of the mean flow.

To linearize the N-S equations (Eqs.1-3), it is first assumed that the variations in acoustic field are small compared to the corresponding average values. These assumptions can be represented mathematically by

$$\mathbf{v} = \mathbf{v_0} + \mathbf{v}', \qquad p = p_0 + p', \qquad T = T_0 + T', \qquad \rho = \rho_0 + \rho_0(\beta_T p' - \alpha_p T') \tag{12}$$

Where, $\alpha_p = \frac{1}{c_0}\sqrt{\frac{C_P(\gamma-1)}{T_0}}$ is the coefficient of thermal expansion and the isothermal compressibility (β_T) is computed from $\frac{1}{\rho_0}\frac{\gamma}{c_0^2}$. c_0 and γ denote the speed of sound and ratio of specific heats, respectively. Note that, T_0, ρ_0, $\mathbf{v_0}$ and p_0 are computed from either DNS or SST-RANS simulation at the first step. By considering Eq. (12) in full N-S equations (Eqs. 1-3), and by transforming the system of equations to the frequency domain via a Fourier transform, the time derivatives are replaced by $i\omega$ as follows,

$$i\omega\rho + \nabla\cdot(\rho\mathbf{v_0} + \rho_0\mathbf{v}) = 0 \tag{13}$$

$$\begin{aligned}\rho_0(i\omega\mathbf{v} + (\mathbf{v}\cdot\nabla)\mathbf{v_0} + (\mathbf{v_0}\cdot\nabla)\mathbf{v}) + \rho(\mathbf{v_0}\cdot\nabla)\mathbf{v_0} = -\nabla\cdot p\mathbf{I} + \\ \nabla\cdot(\mu(\nabla\mathbf{v} + (\nabla\mathbf{v})^T) + (\mu_b - \frac{2}{3}\mu)(\nabla\cdot\mathbf{v})\mathbf{I})\end{aligned} \tag{14}$$

$$\begin{aligned}\rho_0 C_p(i\omega T + \mathbf{v}\cdot\nabla T_0 + \mathbf{v_0}\cdot\nabla T) + \rho C_p\mathbf{v_0}\cdot\nabla T_0 - \alpha_p T_0(i\omega p + \\ \mathbf{v}\cdot\nabla p_0 + \mathbf{v_0}\cdot\nabla p) - \alpha_p T(\mathbf{v_0}\cdot\nabla p_0) - \nabla\cdot(K\nabla T) = 0\end{aligned} \tag{15}$$

where, i is the imaginary unit $i^2 = -1$, and ω is the angular frequency and should not be confused with specific dissipation rate in the turbulent model in CFD solver. The transformation of the equation to frequency domain allows elimination of typical difficulties of this approach in time domain Now the acoustic field ($\mathbf{v}', p', T', \rho'$ variables) can be obtained by solving the LNSE in the frequency domain.

As it is already noted, often advantageous to build an analysis based on linking acoustically characterized sub-models (1D network modeling). This approach is efficient if some part of the system communicates with the rest of it via small number of variables (ports) and in each port the number of exchange variables is also small. Typical situation is then the selected subsystem has only one acoustic port at the upstream side and one at the downstream side of it. If the acoustic field at the ports can be treated as planar waves, then two exchange variables at each of the ports are sufficient to describe the input-to-output properties of the element. The acoustic properties of elements can be described in terms of the respective (exchangeable) transfer and scattering matrix [14]. The scattering matrix expressed in terms of Riemann invariants provides a convenient base for the 1-D network modeling. Within this approach, the down and upstream traveling waves are expressed as a linear combination of primitive acoustic variables p' and u' as the following,

$$f = \frac{k_-}{k_- + k_+}\left(\frac{p'}{\rho c} + \frac{k_0 u'}{k_-}\right), \qquad g = \frac{k_+}{k_- + k_+}\left(\frac{p'}{\rho c} - \frac{k_0 u'}{k_+}\right); \tag{16}$$

where, $k_\pm = \frac{k_0}{1 \pm M_\infty}$ and $k_0 = \frac{\omega}{c}$ represent convective wave number and principal wave number, respectively. As Schematically shown in 1, one can relate the outgoing waves (g_1, f_2) to the incoming characteristic (f_1, g_2) as follows,

$$\begin{bmatrix} g_1 \\ f_2 \end{bmatrix} = \begin{bmatrix} S_{11} & S_{12} \\ S_{21} & S_{22} \end{bmatrix} \cdot \begin{bmatrix} f_1 \\ g_2 \end{bmatrix} + \begin{bmatrix} g_1^s \\ f_2^s \end{bmatrix}, \tag{17}$$

where, the scattering matrix S describes how incoming sound waves are transmitted and reflected by the element. It is called the dependent part of The coefficients S_{11} and S_{22} represent the complex-valued reflection seen from the upstream and downstream, respectively. The coefficients S_{12} and S_{21} denote the complex-valued transmission from upstream to downstream and vice versa. On the other hand, the entries g_1^s and f_2^s are called the independent part, which describes the independent sound (e.g. flow induced noise). Characterization of the independent part is out of scope of the current study and is neglected. To determine the four entries in the scattering matrix, two independent acoustic measurements are needed, denoted I and II [11, 14]. In numerical experiments, this is usually accomplished using a version of the two-source location method in addition to defining perfectly matched layers (PMLs) on the left and right sides of the computational domain to minimize the contribution of spurious signal. The elements of $\mathbf{S}$ can then be calculated using the following representation [11]:

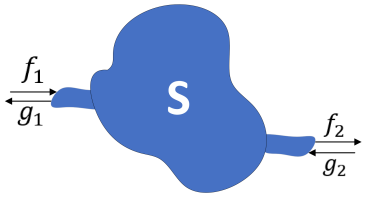

Figure 1: A generic acoustic network element.

$$\mathbf{S} = \begin{bmatrix} \overbrace{S_{11}}^{R_1} & \overbrace{S_{12}}^{T_{2\to1}} \\ \underbrace{S_{21}}_{T_{1\to2}} & \underbrace{S_{22}}_{R_2} \end{bmatrix} = \begin{pmatrix} f_2^I & f_2^I \\ g_1^I & g_1^{II} \end{pmatrix} \begin{pmatrix} f_1^I & f_1^{II} \\ g_2^I & g_2^{II} \end{pmatrix}^{-1} \tag{18}$$

more details about the two-source location method and plane wave decomposition can be found in [11, 14].

3. RESULTS & DISCUSSION

To validate the ssCFD-LNSE method, two test cases are investigated. First, the results of modeling within the ssCFD-LNSE method is compared with experimental data taken from the literature for a cold 2D HEX, followed by a comparison with the CFD-SI approach for a hot 2D Hex. These benchmark problems allow a detailed analysis of the properties of the current methodology. In section 3.2 and 3.3, the performance of the method is investigated for a realistic hot 2D HEX in laminar and turbulent flow, respectively.

3.1. Validation of solver

Test case 1: 2D cold HEX in turbulent flow. To validate the current ssCFD-LNSE solver in the turbulent flow, we consider a test case that commonly has been used in the literature [7, 10, 12] according to Figure 2. In the CFD simulation, (i) the velocity is prescribed at the inlet of the duct (RHS of the computational domain); (ii) the symmetric (slip) boundary condition is applied at the top and bottom of duct wall. (iii) The non-slip boundary condition is applied together with the wall functions at $y^+ \approx 1$ on the two half cylinders. (iv) An outflow pressure boundary condition is also applied at the outlet of the channel. In the LNSE simulation, (v) Non-reflecting zones known as Perfectly matched layer (PML) at the inlet and outlet are considered to minimize acoustic reflections of boundaries. The steady-state mean flow is simulated using a compressible Reynolds-Averaged Navier-Stokes (RANS) solver with the SST turbulence model and considering the wall distance initialization for y^+. While the mean flow field is simulated, the perturbed field is solved using the equations (13-15).

In Figure. 3 comparison of the scattering coefficients obtained from ssCFD-LNSE with the

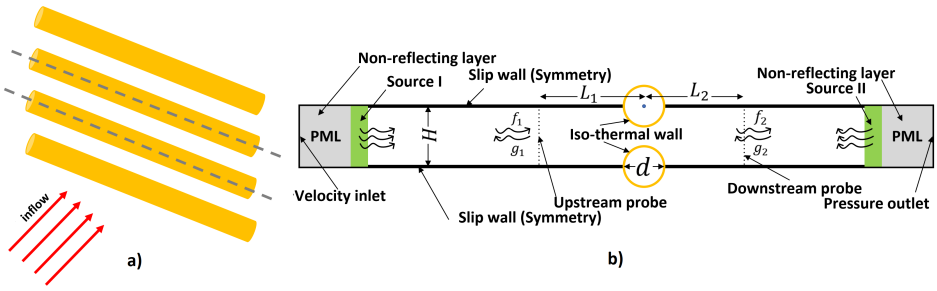

Figure 2: a) Sketch of three-dimensional tube rows with the cross-flow. b) A non-scaled schematic of the two-dimensional (2D) numerical geometry of the tubes-rows HEX.

experimental data shows good agreement in magnitude. To get a better insight into the effect of the mean flow, the results of modeling using Helmholtz equation (acoustic propagation in the absence of inflow) are also shown in the graph. The phases of S_{12}, S_{21} and S_{22} exhibit satisfactory agreement, even though the phase of upstream reflection coefficient $\angle S_{11}$ show a distinct discrepancy between the numerical predictions and the measurements (in spite of the fairly good general trend). One possible reason for this discrepancy could be the presence of non-planer wave effects in the location of pressure measurement by microphones. If this is the case, the scattering coefficients are not independent of the downstream probes. The common way to solve this problem is to measure/record acoustic quantities far enough downstream that the sound wave becomes a plane wave again.

Test case 2: a 2D HEX in laminar hot inflow. Figure 4 shows a comparison between the current method and the method used in [10]. The authors modeled the aeroacoustic response of the tube array, shown in Figure 2, using a quasi-steady-state approach, and the heat transfer across the heat exchanger assumed to be the heat sink. To obtain the latter, they performed transient numerical simulations along with system identification (SI) to obtain the transfer function of the heat exchanger. Apart from a minor difference in the $|S_{12}|$ term, the result is a confirmation that the ssCFD-LNSE

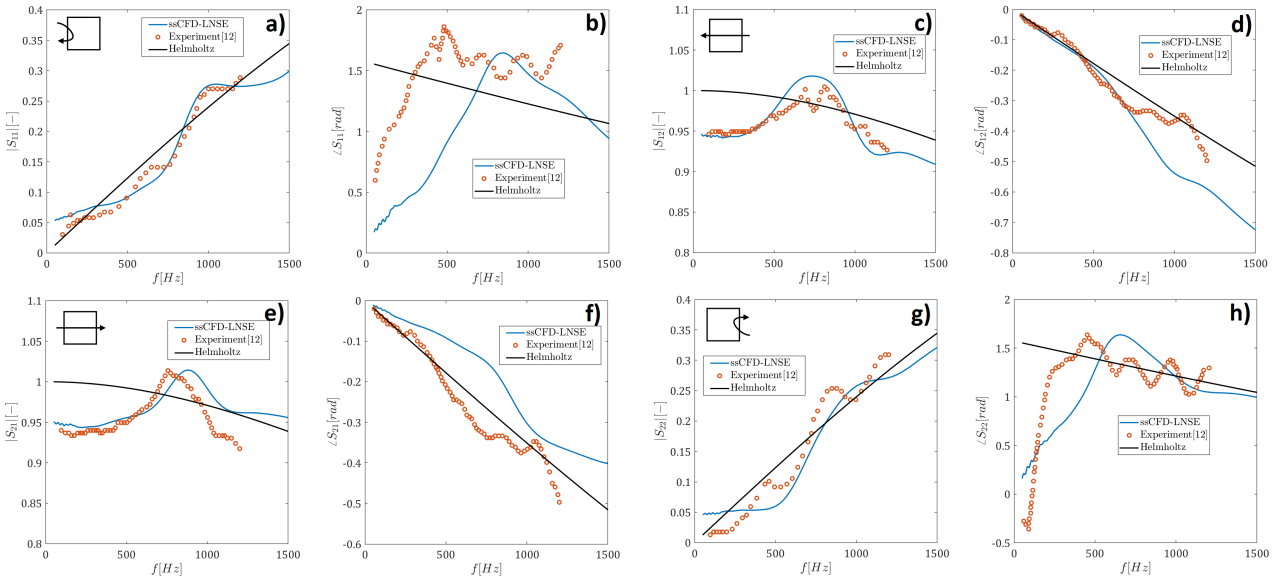

Figure 3: Magnitude and phase of the scattering coefficients for cold turbulent inflow, where $H = 17.2$ mm, $u_\infty = 6.1$ m/s, $R = 5.9$ mm, $L_1 = -R$, $L_2 = R$, $d = 2R$.

solver can accurately model a generic HEX directly from the principle of the two-source method without additional simplification or taking other actions e.g. obtaining TF of HEX.

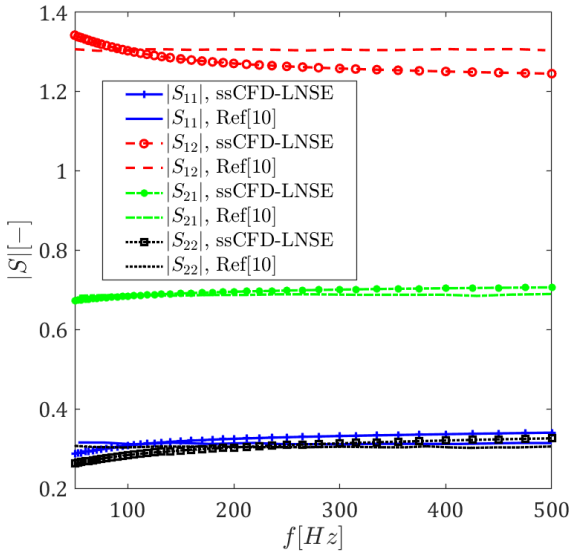

Figure 4: Magnitude and phase of the scattering coefficients for laminar hot flow, where $H = 3.3$ mm, $R = 1.5$ mm, $T_\infty = 1500$ K, $u_\infty = 0.5$ m/s, $T_{hex} = 340$ K.

3.2. A laminar hot HEX

Let us now take a closer look at the results of the ssCFD-LNSE solver for laminar flow. Figure 5 a) shows the mean flow at steady state at the given inflow condition. It can be observed that the velocity increases near the HEX due to geometric contraction. Further downstream, the flow is again the undisturbed channel flow, but the velocity becomes lower than the inflow velocity due to mass conservation accompanied by temperature decreases (see Figure 5b). The variation of the acoustic variables can be visualized in the computational domain using the current method to check the validity of the plane wave assumption. Figure 5 shows a complete propagation of the plane waves in the whole area, since no strong jet flow is formed after the area of contraction expansion (HEX). Figure 6 is

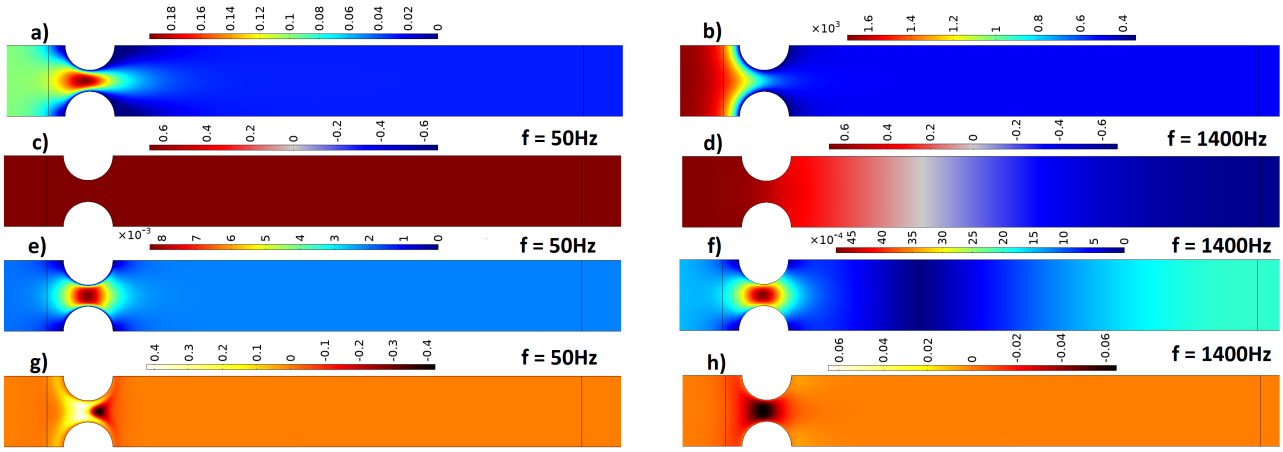

Figure 5: contour plots for laminar inflow, where $H = 17.2$ mm, $R = 6$ mm, $T_\infty = 1700$ K, $u_\infty = 0.1$ m/s, $T_{hex} = 340$ K. a) Velocity magnitude. b) Temperature. c,e,g) acoustic pressure, velocity and entropy, respectively at $f = 50$ Hz. d,f,h) acoustic pressure, velocity and entropy, respectively at $f = 1400$ Hz.

shown the effect of inflow velocity on scattering coefficients. The difference in acoustic impedance of the medium ($\Delta z = \rho_2 c_2 - \rho_1 c_1$) becomes smaller as the inflow velocity increases, causing the reflection coefficients ($|S_{11}|$) to decrease, even though the trend is reversed for the phase of S_{11}. On the other hand, the Figures 6 c,d) show that the larger part of the incoming waves is transmitted at higher inflow velocity, while the phase becomes smaller with increasing inflow velocity. Figure 7

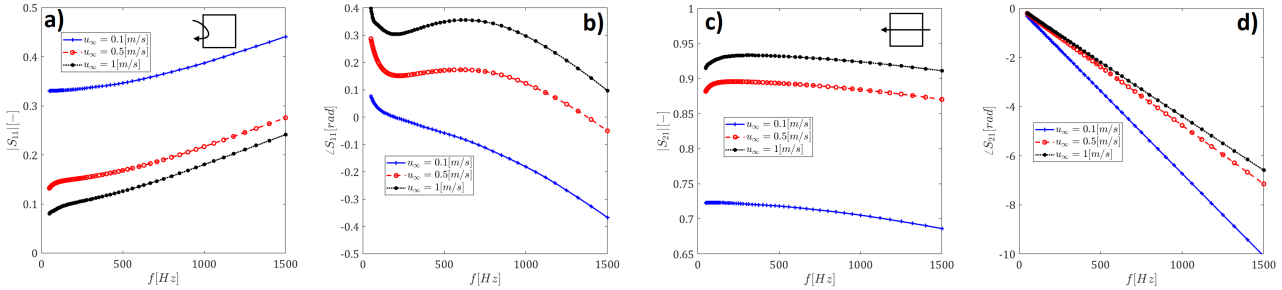

Figure 6: Effect of inflow velocity on the scattering coefficients, where $H = 17.2$ mm, $L_1 = 40$ mm, $L_2 = 0.45$ m, $T_\infty = 1700$ K, $T_{hex} = 340$ K, $R = 6$ mm, $d = 2R$.

includes a comparison of the magnitude and phase of S_{11} and S_{12} for different contraction-expansion gaps ($\delta = H - d$). The magnitude of the upstream reflection coefficient S_{11} increases with decreasing contraction-expansion gap, but this effect on the phase is relatively small, except in the mid-frequency range. On the other hand, the effect on the phase of the transmission coefficient S_{12} is considerable.

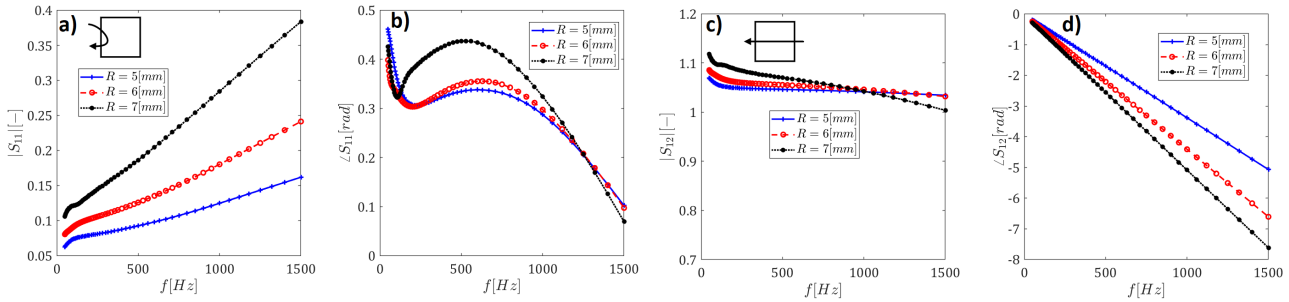

Figure 7: Effect of contraction-expansion gap (δ) on the scattering coefficients, where $H = 17.2$ mm, $L_1 = 40$ mm, $L_2 = 0.45$ m, $T_\infty = 1700$ K, $u_\infty = 1$ m/s, $T_{hex} = 340$ K, $d = 2R$, $\delta = H - d$.

3.3. A turbulent hot HEX

We now consider turbulent hot flow, which gives us insight into the scattering properties of the hot configuration in the turbulent regime. Figures 8 (a, b) show the contour of the mean flow and temperature at the given inflow condition. The strong jet flow near the downstream side is caused by the contraction-expansion within the HEX geometry, where the velocity increases by more than three times the inlet velocity. In contrast to the laminar flow, where a significant temperature drop is observed (see Figure 5 b)), the temperature variation within the HEX is quite small in the turbulent flow.

Figures 8 (c, d) show a plane wave acoustic pressure at the given frequency. The modeling shows that the incident acoustic velocity interacts with the shear layer and forms a jet flow that causes vortex shedding at the downstream side of the HEX. The vortices are convected by the mean flow with a certain velocity. Figures 8 (e,f) show that as the frequency increases, the wavelength becomes shorter as well as more number of the smaller size vortices are seen within the same jet flow. The observed non-planar phenomenon (i.e., acoustic vortex motion) is attenuated at shorter distances from the HEX. Considering the momentum equation (Eq.14), it can be seen that the speed of sound in the limit of zero frequency strongly depends on the mean flow and its gradient, therefore a similarity between the mean flow and the acoustic particle velocity at low frequency is found. As the frequency increases, the effect of the unsteady term ($\rho_0 i\omega \mathbf{v}'$) becomes dominant, and after a short distance from the jet flow, a plane acoustic wave again can be seen.

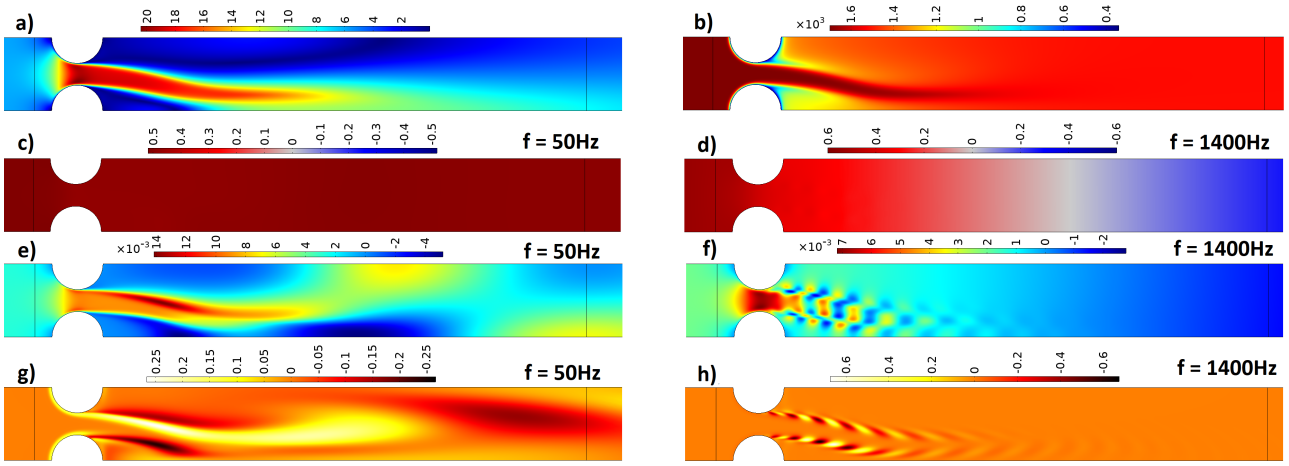

Figure 8: contour plots for turbulent inflow , where $H = 17.2\ mm$, $R = 6\ mm$, $T_\infty = 1700\ K$, $u_\infty = 6\ m/s$, $T_{hex} = 340\ K$. a) Velocity magnitude. b) Temperature. c,e,g) acoustic pressure, velocity and entropy, respectively at $f = 50\ Hz$. d,f,h) acoustic pressure, velocity and entropy, respectively at $f = 1400\ Hz$.

Figures 8 (g,h) present the acoustic entropy, defined as $s'/c_v = p'/p_0 - \gamma\rho'/\rho_0$, at the given frequency. The difference between the entropy wave at low frequency and at high frequency can be explained in the similar way. In addition, it should be noted that a relatively strong non-plannar wave can also be observed in the acoustic pressure contour in the mid-frequency range as the nature of near field acoustics. Our preliminary study has shown that there could be a connection between this non-Plannar wave and the independent aeroacoustic sources (i.e., the g_1^s and f_2^s entries in Eq.17). This is not the subject of the current work, and we leave this question open for the future.

Figure 9 (a,b) shows the magnitude and phase of the S_{11} coefficient at different inflow velocities. The effect of the inflow velocity in a turbulent flow on the phase of the scattering coefficient is larger than the magnitude. However, it can be seen that the magnitude increases with rising inflow velocity up to a certain frequency and then the trend reverses. This phenomenon can also be explained by a closer look at the momentum equation (Eq. 14) and is already explained in Figure 8 (e,f). The effect of the contraction-expansion gap (gap at the neck of the HEX) on S_{11} is evaluated in Figure 9 (c,d).

As mentioned earlier, this entry describes the reflection coefficient, and it increases with decreasing contraction-expansion gap due to the stronger contraction-expansion within the HEX.

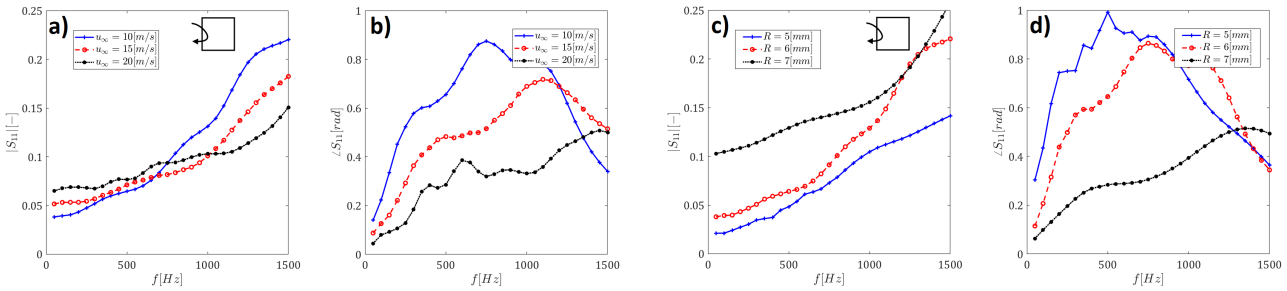

Figure 9: a,b) Effect of inflow velocity, c,d) Effect of contraction-expansion gap (δ) on the scattering coefficients in turbulent inflow, where $H = 17.2\ mm$, $R = 6\ mm$, $T_\infty = 1700\ K$, $u_\infty = 10\ m/s$, $T_{hex} = 340\ K$.

4. CONCLUSIONS

The numerical work is performed based on the ssCFD-LNSE approach performed in the frequency domain. The mean flow field is first simulated using either DNS for laminar flow or SST-RANS for turbulent flow. The acoustic field is then calculated by solving the LNSE. The mean flow is assumed to be stationary, but no other assumptions are made. In the domestic boiler application, where the hot post-flame flow becomes cold within the HEX and exits the boiler through a stack, we can acoustically characterize the HEX along with the stack by placing a downstream probe at the end of the stack. This allows us to use a fairly coarse mesh for the simulation, since the high resolution is not required to resolve small eddies downstream of the HEX. Therefore, this method proves to be efficient for modeling any acoustically passive element, even with complex geometry, fluid dynamics and heat transfer phenomena. The main results of our current study can be summarized as follows:

- Scattering coefficients depend strongly on the acoustic impedance jump of the medium ($\Delta z = \rho_2 c_2 - \rho_1 c_1$). Therefore, for the considered generic HEx model, the effect of mean inflow velocity on the modulus of scattering properties becomes smaller at higher inflow velocity.
- It was noted that the upstream reflection coefficient (S_{11}) appears to be the scattering matrix element that is most sensitive to the imposed mean inflow.
- A slight change in the contraction-expansion gap can cause a significant change in the scattering matrix. This opens the door to new possibilities, performing parametric designs to affect the stability of power generation units equipped with heat exchangers.

ACKNOWLEDGEMENTS

This research benefited from a full financial support from Orkli, S.Coop in Spain and the authors gratefully acknowledge it. We would also like to show our gratitude to Ignacio Sanchez and Mikel Ocana at the company who worked alongside us and provided insight, expertise and technical support that greatly assisted the research.

REFERENCES

[1] Wolfgang Polifke and C Schram. System identification for aero-and thermo-acoustic applications. *Advances in Aero-Acoustics and Thermo-Acoustics. Van Karman Inst for Fluid Dynamics., Rhode-St-Genèse, Belgium*, 2010.

[2] Margaret C Quinn and MS Howe. The influence of mean flow on the acoustic properties of a tube bank. *Proceedings of the Royal Society of London. A. Mathematical and Physical Sciences*, 396(1811):383–403, 1984.

[3] XY Huang, Maria Heckl, et al. Transmission and dissipation of sound waves in tube bundles. *Acta Acustica united with Acustica*, 78(4):191–200, 1993.

[4] Victor Twersky. On the scatttering of waves by an infinite grating. *IRE Transactions on Antennas and Propagation*, 4(3):330–345, 1956.

[5] Victor Twersky. On scattering of waves by the infinite grating of circular cylinders. *IRE Transactions on antennas and propagation*, 10(6):737–765, 1962.

[6] AP Dowling and IJ Hughes. Sound absorption by a screen with a regular array of slits. *Journal of Sound and Vibration*, 156(3):387–405, 1992.

[7] Aswathy Surendran, Maria A Heckl, Luck Peerlings, Susann Boij, Hans Bodén, and Avraham Hirschberg. Aeroacoustic response of an array of tubes with and without bias-flow. *Journal of Sound and Vibration*, 434:1–16, 2018.

[8] Dirk Ronneberger. *Experimentelle Untersuchungen zum akustischen Reflexionsfaktor von unstetigen Querschnittsänderungen im einem luftdurchströmten Rohr*. PhD thesis, Georg-August-Universität Göttingen, 1967.

[9] Gerardus Carolus Johannus Hofmans. Vortex sound in confined flows. *Ph. D. Thesis*, page 431, 1998.

[10] Aswathy Surendran, Maria A Heckl, Naseh Hosseini, and Omke Jan Teerling. Passive control of instabilities in combustion systems with heat exchanger. *International Journal of Spray and Combustion Dynamics*, 10(4):362–379, 2018.

[11] Axel Kierkegaard, Susann Boij, and Gunilla Efraimsson. A frequency domain linearized navier–stokes equations approach to acoustic propagation in flow ducts with sharp edges. *The Journal of the Acoustical Society of America*, 127(2):710–719, 2010.

[12] Wei Na. *A Linearized Navier-Stokes Equations Methodology for Aeroacoustic and Thermoacoustic Simulations*. PhD thesis, KTH Royal Institute of Technology, 2021.

[13] Florian R Menter. Two-equation eddy-viscosity turbulence models for engineering applications. *AIAA journal*, 32(8):1598–1605, 1994.

[14] Manchar Lal Munjal. *Acoustics of ducts and mufflers with application to exhaust and ventilation system design*. John Wiley & Sons, 1987.